Effects of Electrothermal Vortices on Insulator-Based Dielectrophoresis for Circulating Tumor Cell Separation

Arian Aghilinejad [1], Mohammad Aghaamoo [2], Xiaolin Chen [1], and Jie Xu[3]

[1] Department of Mechanical Engineering, Washington State University, Vancouver, WA, USA

[2] Department of Biomedical Engineering, University of California, Irvine, CA, USA

[3] Department of Mechanical and Industrial Engineering, University of Illinois at Chicago, Chicago, IL, USA

Correspondence: Jie Xu, PhD

Phone: 312-355-1788

Fax: 312-413-0447

Email: jiexu@uic.edu

Abbreviations:

CTC: Circulating Tumor Cell; iDEP: insulator-based dielectrophoresis; JH: Joule Heating; ET: Electrothermal

Total Word count:

Abstract

Insulator-based dielectrophoresis (iDEP) is known as a powerful technique for separation and manipulation of bioparticles. In recent years, iDEP designs using arrays of insulating posts have shown promising results towards reaching high-efficiency bioparticle manipulation. Joule heating (JH) and electrothermal (ET) flows have been observed in iDEP microdevices and significantly affecting their performances. In this research, we utilize mathematical modeling to study, in detail, iDEP technique and the effects of JH and ET flow on device performance and propose our separation scenario for selective trapping of circulating tumor cells (CTCs). For this purpose, a robust numerical model is developed to calculate the distribution of electric and fluid flow fields in the presence of JH and ET flow, and predict the cells' trajectory inside the system. Our results indicate that JH not only gives rise to the temperature rise in the system, but also may alter the iDEP separation scenario designed in advance by inducing ET vortices that affect the cell's trajectory. To investigate the impact of JH-induced ET flow characteristics and vortex generation on separation efficiency, we introduce a dimensionless force ratio encompassing the effects of electrical field, drag forces, JH, and ET flow. Interestingly, it was found that ET flows can be used to significantly enhance the separation efficiency, even in higher inlet flow rates. Moreover, the effect of post geometry has been discussed.

Keywords

Circulating Tumor Cell / Dielectrophoresis / Electrothermal flow / Joule Heating

1. Introduction

In recent years, dielectrophoresis (DEP) has emerged as a promising technique for isolation and enrichment of target cells from biological samples. One major application is its use in isolation of circulating tumor cells (CTCs) for both cancer diagnosis and prognosis [1]. DEP working principle is based on using a non-uniform electric field to induce motion in polarizable particles or cells. This technique has been brought into biological applications for the separation of blood cells [3], bacteria [4] and CTCs [2]. Recently, insulator based DEP (iDEP) has gained popularity due to its advantages in fabrication and low cost. In contrast to conventional DEP in which the non-uniform electric field is generated by arrays of electrodes inside the microchannel, iDEP technique utilizes the combination of remote electrodes outside the channel with insulating obstacles within the device to produce the spatial non uniformities in electrical field. This results in the independency of separation efficiency from cells' distance to the electrodes [5]. Previously, there have been different types of insulating obstacles studied for iDEP such as single insulating constrictions [6], serpentine microchannel [7] and arrays of insulating posts [8]. Because of relatively uniform presence of DEP forces along the microchannel, using arrays of microposts have become popular recently. Additionally, there are several studies investigating the effects of different parameters such as the spacing and shapes of the insulating posts [22, 23]. Even though iDEP works with both DC [9] and AC [10] electric field, iDEP designs with AC electric field add applied electric field frequency as an extra degree of freedom to the design to manipulate cells [11]; a unique feature that empowers separation of cells with minor differences in their intrinsic properties.

Although iDEP is a reliable and efficient method for manipulating particles in lab-on-a-chip devices, Joule heating (JH) is a major concern when dealing with biological applications [12]. This phenomenon, which is a result of resistive power dissipation in conductive mediums, may impact device performance due to variation in the medium's temperature-dependent properties, i.e. conductivity, permittivity, viscosity, and density [13]. As a result of the temperature changes due to the JH, local gradients in conductivity and permittivity would be created in the solution, and consequently cause bulk fluid forces and fluid motion, known as electrothermal (ET) flow. Studying and utilizing ET flow in particle manipulation has been previously conducted for DEP-based devices with embedded electrodes inside the microchip [14].

More recently, JH and induced ET flows have also been investigated in the context of iDEP mostly on single constriction microchannels. Hawkins and Kirby modeled JH and the corresponding ET flows in a single constriction iDEP device, with a DC-offset, and an AC electric field [15]. Their results demonstrated the presence of ET vorticities around the channel constriction, enhancing entrapment by affecting particles' deflection and decreasing fluid velocity. Sridharan et al. used both experimentation and numerical simulations to study the effects of JH on electroosmotic flow in an iDEP microdevice, i.e. a constriction microchannel [16]. They found that JH-induced ET flow circulations form near channel constrictions and recirculation vortices exist at AC voltages from 200V to 600V. This group also experimentally investigated the JH on the electrokinetic particle transport and manipulation and has developed a transient 3D numerical model to study the JH-induced ET flows on microdevice [17, 18]. Recently, Kale et al. has investigated the effects of JH and ET streamlines experimentally by introducing the particle trapping number in single constriction microchannel [19]. Prabhakaran et al. has recently observed ET fluid circulations in polymer microfluidic chip and reported the presence of the fluid circulations at 500V AC and above [21]. Studying iDEP device with arrays of insulating posts, Gallo-Villanueva et al. observed reduced particle trapping efficiency due to the decrease in electric field gradient because of JH in the posts' region [20].

Despite the valuable research conducted on JH and ET flow in microfluidics devices, few has focused directly on applications related to separation of biological samples, specifically CTC separation. Moreover, the literature still lacks a thorough study that provides a detailed design guideline based on JH and ET flow for iDEP-based technique. To address these issues, here, we define the problem as to study iDEP with arrays of insulating posts for trapping-based CTC separation. Specifically, we utilize numerical simulation to study extensively how JH and ET flow affect the system performance and what critical design considerations should be taken into account in decision makings. To achieve this goal, we develop a fully coupled electro-thermo-fluid numerical model to investigate the relationship between the device operation parameters and the modelled JH and ET flows. In addition, particle tracing model is coupled with the developed numerical model to further predict the trajectories of cells in the device. Utilizing such a numerical model platform, we study in detail how different operation parameters such as electric field, inlet velocity, medium properties, and post geometries contribute to JH and ET flows. This study is among the first to focus on the effects of Joule Heating and ET flows in iDEP designs for separation of CTCs from blood cells. It is worth noting that although the present research focus on iDEP with arrays of insulating posts, the developed numerical platform is easily extendible to any iDEP designs for bioparticle separations.

2. Theory and Principle

2.1. Governing Equations

The Dielectrophoresis (DEP) arises from the action of the applied electric field on the dipole moment it induces in an object. In the presence of a non-uniform electric field, the electric forces acting on each side of the induced dipole are unequal, causing a net dielectrophoresis force to act on the object. Induced polarization is the underlying phenomenon on which the DEP technique is based. Charges have to be induced to guarantee the continuity of the normal component of total current density in a conductivity gradient, a phenomenon called Maxwell-Wagner interfacial charge relaxation or structural polarization. The dielectrophoretic force is used here to separate the cells based on their differences in dielectric properties. The time average of this force in an inhomogeneous and time-varying electrical field *E*, is proportional to the cell volume, as shown by the following equation:

$$\langle \boldsymbol{F}_{DEP} \rangle = 2\pi\varepsilon_m r^3 Re(K_{CM}) \nabla |\boldsymbol{E}|^2 \quad (1)$$

where ε_m is the permittivity of the medium, r the radius of the cell, and $Re(K_{CM})$ is the real part of the Clausius-Mossotti factor defined as

$$K_{CM} = \frac{\bar{\varepsilon}_{cell} - \bar{\varepsilon}_m}{\bar{\varepsilon}_{cell} + 2\bar{\varepsilon}_m} \quad (2)$$

where $\bar{\varepsilon} = \varepsilon - j\frac{\sigma}{\omega}$ is the complex permittivity considering the permittivity and conductivity of the cell and the medium and also angular frequency (ω) of the electrical field. Clausius-Mossotti factor varies between -0.5 to 1 depending on the balance of complex permittivity of the particle and medium. When $\bar{\boldsymbol{\varepsilon}}_{\boldsymbol{p}} > \bar{\boldsymbol{\varepsilon}}_{\boldsymbol{m}}$, it means that the cell is more polarizable than the medium, the DEP force would be positive (pDEP) which makes the particles get attracted to the high electric field zones. Conversely, when $\bar{\boldsymbol{\varepsilon}}_{\boldsymbol{p}} < \bar{\boldsymbol{\varepsilon}}_{\boldsymbol{m}}$, the DEP force would be negative (nDEP), meaning particles get forced back from high electric field regions. It is to be mentioned that at specific frequency, called crossover frequency, the Clausius-Mossotti factor would be zero, resulting in no dielectrophoretic force.

In this study, the calculations were performed, using breast cancer cell and white blood cells as a model, in view of the major importance of these cells in biotechnology. The common approach to theoretically model the biological

particles is to use a concentric multi shell model. In this study, single shell model is used to consider the cell's thin membrane effect on its overall dielectric performance [24]. In this model, equivalent cell complex permittivity can be calculated using cytoplasm and membrane complex permittivity $(\overline{\boldsymbol{\varepsilon_{cyt}}}$ and $(\overline{\boldsymbol{\varepsilon_{mem}}})$:

$$\varepsilon_{cell} = \varepsilon_{mem} \frac{\gamma^3 + 2(\frac{\varepsilon_{cyt} - \varepsilon_{mem}}{\varepsilon_{cyt} + 2\varepsilon_{mem}})}{\gamma^3 - (\frac{\varepsilon_{cyt} - \varepsilon_{mem}}{\varepsilon_{cyt} + 2\varepsilon_{mem}})} \tag{3}$$

where $\gamma = \frac{r_{cell}}{r_{cell} - d}$ and d is the cell membrane thickness. The dielectric properties of breast cancer cells and granulocytes are reported by Becker et al. [25] and Yang et al. [26], respectively, and are listed in Table 1.

Table 1.Mechanical and electrical properties of selected cells

Cell type	Tissue	$r(\mu m)$	ε_{mem}	$\sigma_{mem}\ (\frac{S}{m})$	ε_{cyt}	$\sigma_{cyt}\ (\frac{S}{m})$	$d\ (nm)$	Ref.
Granulocytes (WBC)	Blood	4.71	5	1×10^{-6}	65	0.6	4	[26,38]
MDA-231	Breast	6.2	11.75	1×10^{-6}	52	0.62	4	[25,39]

Based on these dielectric properties, the real part of Clausius-Mossotti is plotted with respect to different applied electric field frequency and medium conductivities (Figure 1).

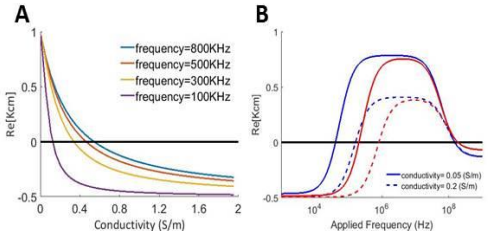

Figure 1. (A) Clausius-Mossoti factor for MDA-231 in different conductivities, (B) The behavior of Breast cancer cell(blue) and White blood cell(red) for different frequencies

According to Figure 1A, by increasing the frequency, the critical conductivity at which the cells change behavior from pDEP to nDEP will be increased. As shown in Figure 1B, MDA-231 and WBC behave differently at different frequencies for two representative conductivities. For the purpose of CTC separation, we take the advantage of such a difference to trap one type of cells while allowing the other ones to pass through the device. To achieve this, if the applied frequency is more than the crossover frequency for MDA-231, pDEP will be applied to CTCs. On the other hand, when the frequency is less than the crossover frequency for white blood cell, it experiences nDEP; hence in this middle range, breast cancer cells would experience pDEP which attracts them to the microposts and possibly results in trapping while white blood cells would experience nDEP. It is worth mentioning that, generally, it is easier to attract particles using pDEP rather than repelling them by nDEP [12]. Furthermore, working in pDEP regime is more straight-forward especially in low conductive mediums [27].

Most of the previous studies approximated medium conductivity dependency to temperature as a linear function [13]. However, Porras et al. demonstrate that it is more accurate to use quadratic equation as [28]

$$\sigma = \sigma_0[1 + P_1(T_{mean} - T_0) + P_2(T_{mean} - T_0)^2] \quad (4)$$

where σ_0 is conductivity at reference temperature (T_0) and parameters P_1 and P_2 were determined experimentally by Porras et al. which here would be $0.02071\frac{1}{K}$ and $4.3\times10^{-5}\frac{1}{K^2}$ respectively.

For the permittivity and viscosity of the medium, same as previous studies, we have [13, 16, 18, 29]

$$\varepsilon(T) = \varepsilon_0(1 + \alpha(T - T_0) \quad (5)$$

$$\mu = 2.761 \times 10^{-3}\exp(\frac{1713K}{T}) \quad (6)$$

where ε_0 is fluid permittivity at reference temperature and α is temperature coefficient of fluid permittivity which is $-0.0046\frac{1}{K}$ in this study. Other properties such as thermal conductivity and heat capacity can be safely assumed as constant as DI water in our study.

2.2. Numerical Model Description

Joule heating modelling with associated ET flows requires coupling three physics: thermal, electric, and fluid flow. In this regard, COMSOL Multiphysics (Fluid Flow, Heat transfer in fluids, and AC/DC) was used to solve for the flow, temperature, and electric fields in the system. Also, we have used particle tracing module in COMSOL Multiphysics to track the trajectory of the bioparticles. The geometry is shown in Figure 2. For calculating flow rates, we assumed the height of the channel as 100 µm.

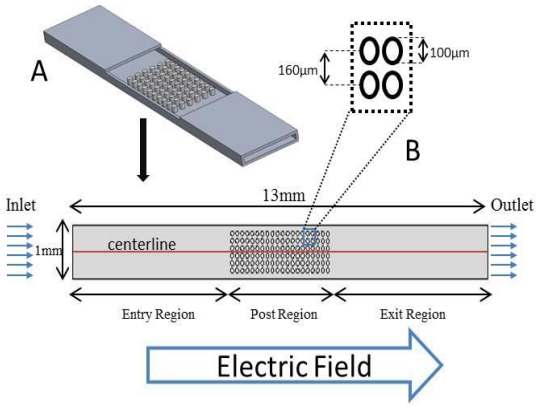

Figure 2. (A) Isometric view of the iDEP device, (B) Geometry of the microchip and design parameters

In order to determine the electric field distribution in the system, the Gauss's law and charge conservation need to be satisfied simultaneously. The electric field $\boldsymbol{E}$ is governed by the following set of equations [24]:

$$\nabla \cdot (\varepsilon \boldsymbol{E}) = \rho_f \tag{7-a}$$

$$\nabla \cdot (\sigma \boldsymbol{E}) + \frac{\partial \rho_f}{\partial t} = 0 \tag{7-b}$$

$$\boldsymbol{E} = -\nabla \phi \tag{7-c}$$

where the medium permittivity $\varepsilon = \varepsilon_0 \varepsilon_r$ with $\varepsilon_0 = 8.854 \times 10^{-12} Fm^{-1}$ and ε_r being the relative medium permittivity, ρ_f is the free charge density, σ is the medium conductivity, t is the time coordinate, and ϕ is the electric potential. Note that the frequency of the AC field used in this study is on the order of kHz, much lower than the charge relaxation frequency ($f_r = \frac{\sigma}{2\pi\varepsilon}$), which is on the order of 10 MHz. At such low frequencies, the frequency effects on the electric displacement will become negligible compared to effects caused by the variation of temperature [34]. As the applied voltage is an AC signal, we use the phasor amplitude of the electric field $\tilde{E}$ and

express $\boldsymbol{E}$ as $\boldsymbol{E}(t) = Re(\tilde{E}e^{j\omega t})$, where *Re* indicates the real part of the complex valued field, ω=2πf is the angular frequency and *j* is the imaginary unit.

The time-averaged temperature field, *T*, is governed by the energy equation, as follows:

$$\rho C_p(\boldsymbol{v} \cdot \nabla T) = \nabla \cdot (k\nabla T) + \sigma\langle \boldsymbol{E^2} \rangle \tag{8}$$

where ρ is the fluid density, C_p is the heat capacity, $\boldsymbol{v}$ is the fluid velocity, k is the fluid conductivity, and the last term corresponds to the power generation source due to Joule heating. Note that σ is the conductivity of the medium and $\boldsymbol{E}$ is the applied electric field.

Finally, the flow field is obtained by solving the Navier-Stokes and continuity equations:

$$\rho\left[\frac{\partial \boldsymbol{v}}{\partial t} + (\boldsymbol{v} \cdot \nabla)\boldsymbol{v}\right] = -\nabla p + \nabla \cdot (\eta \nabla \boldsymbol{v}) + \boldsymbol{f}_E \tag{9-a}$$

$$\nabla \cdot \boldsymbol{v} = 0 \tag{9-b}$$

where $\rho, \boldsymbol{v}, p$ and η are the fluid density, velocity, pressure, and viscosity, respectively. The ET effects appear as a volume force, $\boldsymbol{f}_E$. The general form of this force is:

$$\boldsymbol{f}_E = \rho_f \boldsymbol{E} - \frac{1}{2}\boldsymbol{E}^2\nabla\varepsilon + \frac{1}{2}\nabla\left(\rho\frac{\partial \varepsilon}{\partial \rho}\boldsymbol{E}^2\right) \tag{10}$$

where ρ_f is the free charge density, ε is the medium permittivity, and ρ is the fluid density. For an incompressible fluid, assumed in this study, the last term can be neglected. In the presence of non-uniform electric field, the electric field acts on gradients in permittivity and conductivity produced by non-uniform heating of the fluid, and produces the so-called electrothermal (ET) flow. Such a mechanism for driving electrothermal flow is well explained in Gimsa et al. [34, 37]. Assuming the electric field $\boldsymbol{E} = \boldsymbol{E}_0 + \boldsymbol{E}_1$, where $\boldsymbol{E}_0$ represents the isothermal solution obtained in the absence of gradients and $\boldsymbol{E}_1$ is a small perturbation field caused by temperature variations, we follow the same procedure as the previous work [30, 34, 35, 36, 37] in derivation of the time-averaged ET force per unit volume, $\langle \boldsymbol{f}_E \rangle$, which results in:

$$\langle \boldsymbol{f}_E \rangle = -\frac{1}{2}\left[\left(\frac{\nabla\sigma}{\sigma} - \frac{\nabla\varepsilon}{\varepsilon}\right) \cdot \boldsymbol{E}_0 \frac{\varepsilon \boldsymbol{E}_0}{1+(\omega\tau)^2} + \frac{1}{2}|\boldsymbol{E}_0|^2\nabla\varepsilon\right] \tag{11}$$

where $\tau = \varepsilon/\sigma$ is the charge relaxation time of the medium. In the right-hand side of the above equation, the first term is the Coulomb force due to the conductivity gradient and the second term is the dielectric force due to permittivity gradient. The Coulomb force dominates at low frequencies but vanishes at very high frequencies as it depends on the induced free charge which decays due to charge relaxation inside the fluid at higher frequencies. On the other hand, the dielectric force dominates at high frequencies as it is determined by the polarized bound charge that survives in the high frequency AC field in the presence of a permittivity gradient.

By applying Newton's second law, we can relate the momentum rate to the net forces and therefore the particle trajectory could be determined by

$$m\frac{d(\boldsymbol{v}_{cell})}{dt} = \boldsymbol{F}_{DEP} + \boldsymbol{F}_{drag} \tag{12}$$

where the DEP force is calculated using Eq. (1) and the drag force would be calculated using Stokes drag law as follows:

$$\boldsymbol{F}_{drag} = -6\pi\mu r_{cell}(\boldsymbol{v}_{cell} - \boldsymbol{v}) \tag{13}$$

where μ is the fluid viscosity, r_{cell} is the cell radius and $\boldsymbol{v}_{cell}$ is the cells' velocity and $\boldsymbol{v}$ is the surrounding flow velocity.

Since the characteristic timescale of acceleration phase of the cell's motion is much smaller than the time scale of the variation of the external forces, the inertia force term in Eq. (13) can be omitted. Then, the velocity of the cell due to the surrounding fluid flow and dielectrophoresis is obtained by

$$\boldsymbol{v}_{cell} = \boldsymbol{v} + \frac{\boldsymbol{F}_{DEP}}{6\pi\mu r_{cell}} \tag{14}$$

where $\boldsymbol{v}$ includes the effects of pressure-driven and ET flow on cell trajectory."

To solve these coupled physics, three sets of boundary conditions are required, each corresponding to the specific physic. Table 2 summarizes the boundary conditions used in this study.

Table 2. Summary of the utilized boundary conditions for modeling Joule heating and the corresponding electrothermal flow

Physics	Inlet	Outlet	Channel walls
Electric field	Electric potential ($V = V_{in}$)	Ground ($V = 0$)	Electric insulation ($\boldsymbol{n} \cdot (\sigma \boldsymbol{E}) = 0$)
Fluid flow	Velocity inlet ($\boldsymbol{v} = U_{in}$)	Pressure outlet ($P_{out} = 0$)	No slip ($\boldsymbol{v} = 0$)
Heat transfer	($T = T_0$)	Outflow ($-\boldsymbol{n} \cdot (k\nabla T) = 0$)	Constant Temperature $T = T_0$ (Room Temperature)

3. RESULTS AND DISCUSSION

3.1 Single Constriction iDEP; Validation Study

To validate our developed numerical model, the ET flows, as a result of the non-uniform temperature rise in the channel, were modeled and compared with the experimental and numerical results reported by Sridharan et al. [16] (Figure 3) in the special case of $600V$ pure AC applied voltage.

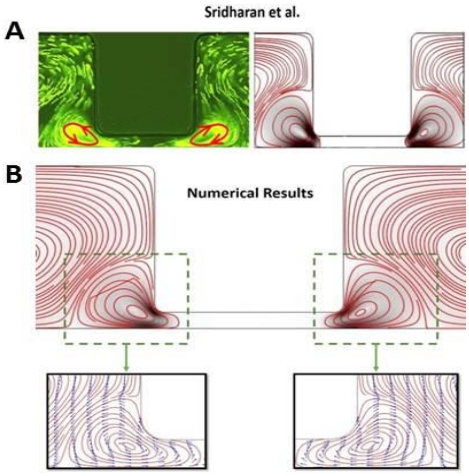

Figure 3. Comparison of the ET flows, as a result of Joule heating, between (a) the work by Sridharan et al., and (b) our developed numerical model. The results shows the capability of our model to predict such phenomenon.

According to the results, our developed numerical model can predict well the ET flows associated with Joule heating. Specifically, as can be seen in Figure 3B, the model can accurately predict the ET vortices with specific circulation directions at inlet and outlet of the microchannel. In order to verify the validity of our simulation, we mainly focus on ET flow pattern and the presence of vortices rather than focusing on magnitude. Sridharen et al. [16] used very high convective heat transfer coefficient in their research in order to be consistent with their experimental results. Therefore comparing the magnitudes would not be helpful to compare our simulation with their results. However, for the current study, the ability of our developed numerical model for predicting both Joule heating and the pattern of ET flows would be sufficient enough.

3.2 Effect of Joule Heating on Temperature, Conductivity and Electrical Field

One of the major phenomena of iDEP technique is the resulting high temperature gradients that would rise due to the high electric field gradients. In this section, we investigate sensitivity of the temperature changes and its effects on gradient electric field squared and conductivity.

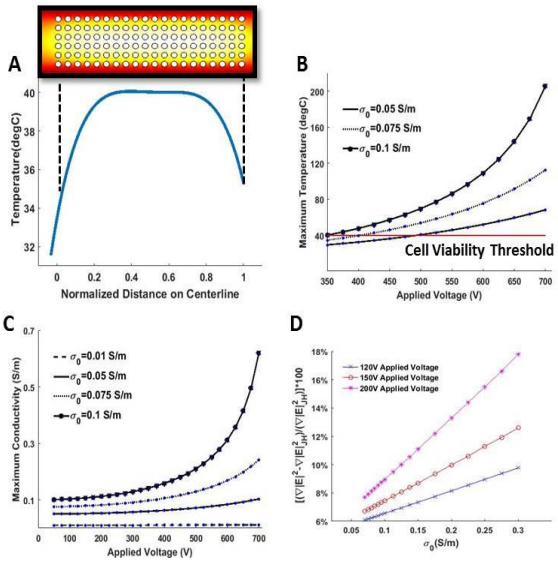

Figure 4. (A) Temperature profile on the centerline of the microdevice, (B) Maximum temperature value for different conductivities for common range of applied voltage in iDEP devices, (C) changes in conductivity due to the temperature gradient inside the microchip, (D) Deviation from the electric field by comparing the gradient of electric field squared when Joule heating is considered ($\boldsymbol{\nabla|E|^2}_{JH}$) neglected ($\boldsymbol{\nabla|E|^2}$).

In Figure 4A, the temperature profile on the centerline of the microchannel is depicted. Due to heat flux boundary condition that is applied on the outlet, the temperature first started to increase to its maximum and after that decrease. Figure 4B depicts the maximum temperature inside the channel for different initial conductivities with respect to the applied voltage. Because our goal in this research was to separate MDA-231 from WBCs, for different conductivities, the frequency should be changed in order to have different type of DEP forces (pDEP and nDEP). Here, we used 20kHz for 0.01S/m, 100kHz for 0.05S/m and 300kHz for 0.075S/m and 0.1S/m conductivities according to Figure 1. These frequencies are in line with the ranges which were previously reported from the experiments done by Das et al. [31]. Note that although we focused on MDA-231 for separation in this study, most

of CTCs behave with a similar trend in the presence of electrical field. Therefore the strategy deployed in this research, can also be applied for different types of CTCs. In Figure 4C, the maximum amount of conductivity for different applied voltages has been presented in different initial conductivities. Note that even for moderate voltage differences, there would be a significant change in conductivity. Such a highly non-linear trend and its effects should be considered in the device behavior specially for trapping the particles as it alters the Classius-Mossoti factor. Figure 4D represents the variation in $\nabla|E|^2$ when JH is considered ($\nabla|E|^2{}_{JH}$) by comparing the values obtained by neglecting JH ($\nabla|E|^2$). The voltages that was used for this study are relatively low to show the significance of deviation even in low applied voltages. By considering these changes in conductivity and electric field gradient due to the temperature in design step, we would be able to predict the influence of the JH on electrical performance of the device.

3.3 Effect of fluid circulations on particle separation

Presence of ET forces inside the device, causes motion in the fluid and create vortices. By modeling the ET force in the microchip, we are able to predict these motions inside of the microchannel. An important implication of these modeling would be to enable the designers to control the effects of ET flow and even using these vortices inside their devices for separation. Figure 5 shows an example case illustrating the JH-induce ET flows in the microchip. Note that the applied voltage is 500V.

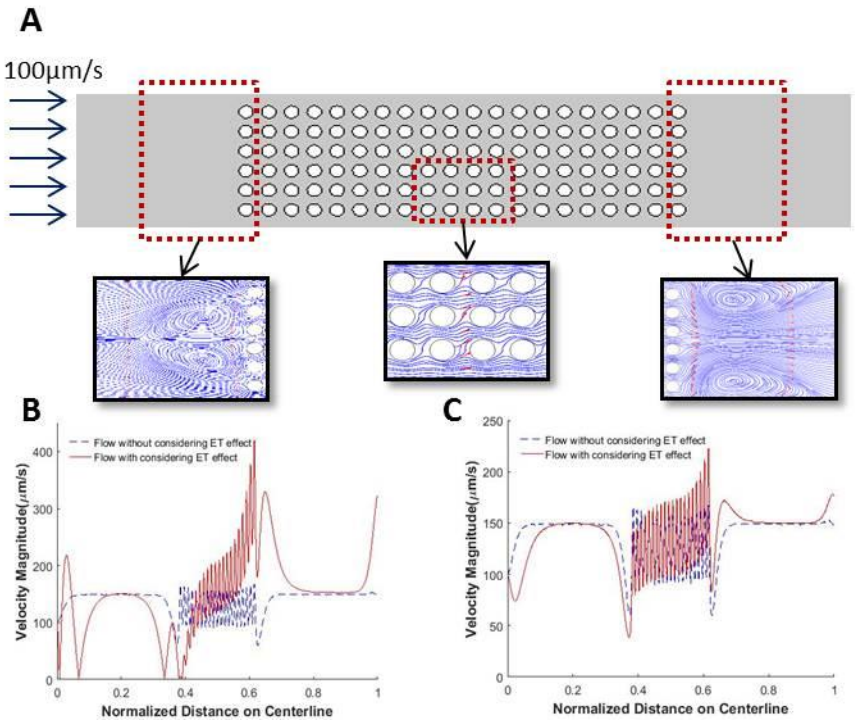

Figure 5. (A) Fluid streamlines inside the microchannel which causes vortices to arise due to electrothermal forces between the posts in a medium with 0.05 S/m conductivity, velocity profile on the centerline (B) For 0.05S/m initial conductivity, (C) For 0.01S/m initial conductivity.

The presence of these vortices could change the regular trajectory of the particles that is predicted by DEP force. For quantitatively showing the effect of these vortices on the main flow, the velocity profile is depicted for two different cases on the centerline: one that considers ET flows and one that neglects ET flows (Figure 5B and 5C). Note that the velocity profile is depicted for two cases as well, one with 0.05S/m conductivity for media and another with 0.01S/m conductivity. It is clear that in lower conductivity, the effect of vortices is negligible (Figure 5C), as previously reported by Gallo-Villanueva et al. [20] while the effect of ET flow on higher conductivity (Figure 5B) is significant. Hereafter, all the further studies are conducted in a medium with 0.05 S/m conductivity because of investigating the effects of ET vortices in physiological range on particle separation. Moreover, according to Figure 1B, it gives us a good range of frequency for separating CTCs from WBCs by applying the appropriate type of DEP force.

To investigate the effect of ET flow on particle trajectory, the trajectory of particles was modeled in the absence and presence of ET flow (Figure 6). The inlet velocity of the flow was 500 um/s which is among the highest inlet velocities for iDEP devices corresponded to 0.1 ml/hr flow rate.

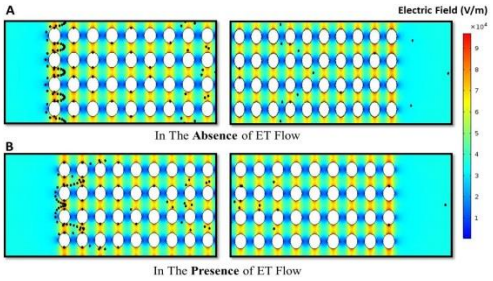

Figure 6. Simulation results obtained using COMSOL Multiphysics software. A comparison of cell (MDA-231) trajectory inside the channel, (A) In the absence of ET flow, (B) In the presence of ET flow. Note that more cells are getting trapped in the presence of ET flow.

Figure 6 represents the difference in particle trapping in the presence of electrothermal flow. Comparing Figure 6A and 6B, presence of ET flow decreases the velocity of particles in the first columns of posts and cause more particles to trap. These simulations could show the significance of the effect of ET flow even in high flow rates. As it could be noticed from Figure 6, in the absence of ET flow, more cells are running away from pDEP traps. Hence, the presence of ET flow could enhance the separation of the cells. With respect to this point that significant temperature rise will threaten the cells' viability, decreasing the cells' residual time in DEP traps compensates this issue while allowing us to take advantage of JH-induced ET vortices. One way to achieve this is to periodically apply perpendicular flow to release the trapped cells [33].

In order to have an accurate and quantified comprehension on how JH and corresponding ET flow would affect cell separation and manipulation, we define a dimensionless force ratio as the ratio between the DEP force and surrounding fluid force. The surrounding fluid force used in the force ratio is caused by the fluid flow due to the ET and pressure gradient effects. This force is calculated based on Eq. (13) considering only the fluid velocity and neglecting the cell velocity. To trap the target cells, higher value of the force ratio experienced by those cells is more desirable. The main advantage of using this parameter is to simultaneously investigate the effects of temperature and

JH on electrical field, conductivity, ET force and velocity which could define the functionality and performance of the design. Using Eqs. (1) and (13), α, the force ratio, would be

$$\alpha = \frac{F_{DEP}}{F_{flow}} = \frac{r_{cell}^2}{3}\left(\frac{\varepsilon_m Re(K_{CM})}{\mu}\right)\frac{\nabla|E|^2}{|v|} \tag{15}$$

Figure 7 represents the force ratio along the centerline of the microchip for $0.02\,\frac{mL}{hr}$, $0.04\,\frac{mL}{hr}$ and $0.06\,\frac{mL}{hr}$ inlet flow rates at 500V applied voltage in 100kHz to trap the MDA-231 cancer cell. In Figures 7-A to 7-C, the effect of ET flow was neglected while in the rests, the ET flow effect was considered.

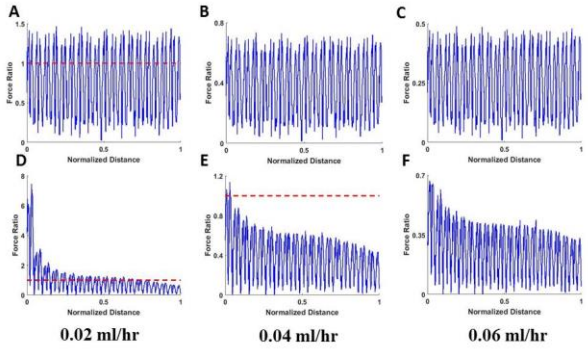

Figure 7. Force ratio for (A,D) 0.02 $\frac{mL}{hr}$, (B,E) 0.04 $\frac{mL}{hr}$ and (C,F) 0.06 $\frac{mL}{hr}$ inlet flow rates and 500V applied voltage for breast cancer cell, In (A,B,C) the effect of ET flow is not considered while in (D,E,F) the ET flow effect is considered. These results show the effect of ET flow which enhances the cell separation by decreasing the cell's velocity.

As it is shown in Figure 7, in all the cases we can achieve higher force ratios by using the ET flow on the centerline of the microchannel at first columns of posts which generally are more important than others for trapping the particles. Due to the presence of ET flow, the magnitude of particles velocity would decrease and cause higher force ratio. Note that force ratio decreases by moving along the centerline toward the outlet. The main reason is the decrease in $\nabla|E|^2$ due to the JH-induced increase in conductivity according to Figure 4. Although the force ratio decreases by moving along the channel, we are still capable to get higher force ratios and trap the cells in first rows.

3.4 Effect of Geometry on fluid circulations

Posts shape and configuration has a direct effect on iDEP trapping efficiency as it affects electric and flow field distribution throughout the system. In Figure 8, the comparison for three basic geometries (circle, diamond, square) has been done.

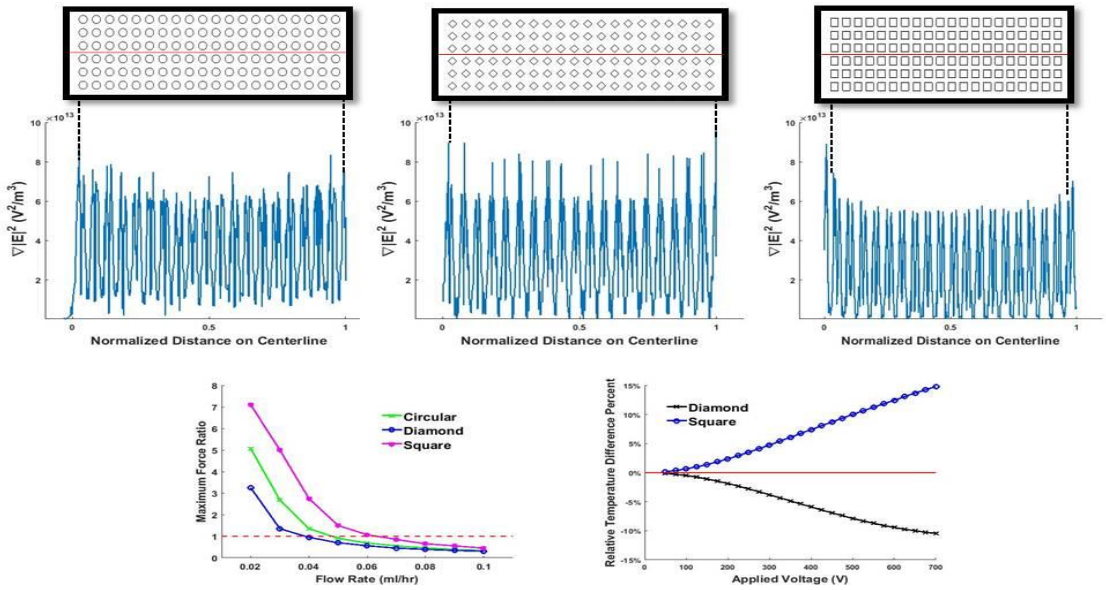

Figure 8. (A, B, C) The gradient of the electric field squared for different geometries along the centerline, (D) Force ratio for different geometries in different flow rates, (E) Temperature rise inside the channel for square and diamond shape microposts relative to circular post.

As shown in Figure 8, $\nabla|E|^2$ for diamond shape post is higher than others as confirmed by previous researches [23, 32]. However, the force ratio for diamond shape microposts is smaller than circular and square shape posts. The reason is that in the presence of the ET vortices inside the channel, the velocity profile is affected by these vortices and shape of microposts has influence on this profile.

As it can be seen from Figure 8D, the maximum force ratio for square shape post is higher than circular and diamond for different inlet flow rates. Note that these values are calculated along the centerline of the device which are located at the largest distance from the posts. This means that trapping of the particles can also happen in values less than one. Figure 8E, compares the temperature rise in square and diamond shape post relative to circular one. The negative percent for diamond represents that in these designs, the temperature rise is less than the circular posts.

These graphs provide a thorough view for using the different shape post depends to the application and can be served as a design guideline. For instance, dealing with particles which are not temperature sensitive, choosing a square shape post would provide higher efficiency and trapping ratio while dealing with temperature sensitive bioparticles such as mammalian cells, diamond would be the best option for keeping the temperature low and does not decrease the force ratio significantly compare to circular posts.

4. Concluding Remarks

Insulator-based dielectrophoresis is an emerging technique and powerful tool for separation and manipulation of bioparticles and cells. Recently, there have been lots of efforts to improve the throughput and performance of this technique. In this study, mathematical modeling was used to simulate the iDEP device performance and design scenario for CTC trapping and separation. To achieve a comprehensive conception toward the technique, JH and induced ET flows was modeled and studied. We developed a fully coupled electro-thermo-fluid numerical tool via temperature dependent material properties and particle tracing modeling to predict the cell trajectory and device performance for different conditions. We also demonstrated that by choosing appropriate frequency, the selective trapping of CTCs become possible, according to its dielectric properties.

The implication of our finding is that ET flows are not always a disadvantage but also can be used to enhance the performance for separation. To quantify this effect, dimensionless force ratio was introduced and utilized in the modeling to show the effects of ET flow and facilitate the comparison between different embedded insulating post geometries which is very critical for iDEP devices. Results show that although the diamond shape posts provide higher electric field gradient, square shape microposts have higher force ratio in presence of ET flows. The systematic research work conducted here provides the fundamental groundwork as well as design guidelines for developing efficient iDEP devices for bioparticles and cells separation.

The authors have declared no conflict of interest.

5. References

[1] Shields, C. W., Reyes, C. D., Lopez, G. P., *Lab on a Chip* 2015, *15*, 1230-1249.

[2] Moon, H. S., Kwon, K., Kim, S. I., Han, H., Sohn, J., Lee, S., Jung, H. I., *Lab on a Chip* 2011, *11*, 1118-1125.

[3] Cheng, I. F., Froude, V. E., Zhu, Y. X., Chang, H. C., Chang, H. C., *Lab on a Chip* 2009, *9*, 3193-3201.

[4] Lapizco-Encinas, B. H., Davalos, R. V., Simmons, B. A., Cummings, E. B., Fintschenko, Y., *Journal of Microbiological Methods* 2005, *62*, 317-326.

[5] Srivastava, S. K., Gencoglu, A., Minerick, A. R., *Analytical and Bioanalytical Chemistry* 2011, *399*, 301-321.

[6] Barbulovic-Nad, I., Xuan, X. C., Lee, J. S. H., Li, D. Q., *Lab on a Chip* 2006, *6*, 274-279.

[7] Zhu, J. J., Tzeng, T. R. J., Hu, G. Q., Xuan, X. C., *Microfluidics and Nanofluidics* 2009, *7*, 751-756.

[8] Shafiee, H., Sano, M. B., Henslee, E. A., Caldwell, J. L., Davalos, R. V., *Lab on a Chip* 2010, *10*, 438-445.

[9] Lapizco-Encinas, B. H., Simmons, B. A., Cummings, E. B., Fintschenko, Y., *Analytical Chemistry* 2004, *76*, 1571-1579.

[10] Nakidde, D., Zellner, P., Alemi, M. M., Shake, T., Hosseini, Y., Riquelme, M. V., Pruden, A., Agah, M., *Biomicrofluidics* 2015, *9*.

[11] Cetin, B., Li, D. Q., *Electrophoresis* 2011, *32*, 2410-2427.

[12] Voldman, J., *Annual Review of Biomedical Engineering*, Annual Reviews, Palo Alto 2006, pp. 425-454.

[13] Xuan, X. C., *Electrophoresis* 2008, *29*, 33-43.

[14] Sin, M. L. Y., Shimabukuro, Y., Wong, P. K., *Nanotechnology* 2009, *20*, 9.

[15] Hawkins, B. G., Kirby, B. J., *Electrophoresis* 2010, *31*, 3622-3633.

[16] Sridharan, S., Zhu, J. J., Hu, G. Q., Xuan, X. C., *Electrophoresis* 2011, *32*, 2274-2281.

[17] Zhu, J. J., Sridharan, S., Hu, G. Q., Xuan, X. C., *Journal of Micromechanics and Microengineering* 2012, *22*, 6.

[18] Kale, A., Patel, S., Hu, G. Q., Xuan, X. C., *Electrophoresis* 2013, *34*, 674-683.

[19] Kale, A., Patel, S., Qian, S. Z., Hu, G. Q., Xuan, X. C., *Electrophoresis* 2014, *35*, 721-727.

[20] Gallo-Villanueva, R. C., Sano, M. B., Lapizco-Encinas, B. H., Davalos, R. V., *Electrophoresis* 2014, *35*, 352-361.

[21] Prabhakaran, R. A., Zhou, Y. L., Patel, S., Kale, A., Song, Y. X., Hu, G. Q., Xuan, X. C., *Electrophoresis* 2017, *38*, 572-579.

[22] Mohammadi, M., Zare, M. J., Madadi, H., Sellares, J., Casals-Terre, J., *Analytical and Bioanalytical Chemistry* 2016, *408*, 5285-5294.

[23] LaLonde, A., Romero-Creel, M. F., Lapizco-Encinas, B. H., *Electrophoresis* 2015, *36*, 1479-1484.

[24] Morgan, H., Sun, T., Holmes, D., Gawad, S., Green, N. G., *J. Phys. D-Appl. Phys.* 2007, *40*, 61-70.

[25] Becker, F. F., Wang, X. B., Huang, Y., Pethig, R., Vykoukal, J., Gascoyne, P. R. C., *Proc. Natl. Acad. Sci. U. S. A.* 1995, *92*, 860-864.

[26] Yang, J., Huang, Y., Wang, X. J., Wang, X. B., Becker, F. F., Gascoyne, P. R. C., *Biophys. J.* 1999, *76*, 3307-3314.

[27] Aldaeus, F., Lin, Y., Roeraade, J., Amberg, G., *Electrophoresis* 2005, *26*, 4252-4259.

[28] Porras, S. P., Marziali, E., Gas, B., Kenndler, E., *Electrophoresis* 2003, *24*, 1553-1564.

[29] Knox, J. H., McCormack, K. A., *Chromatographia* 1994, *38*, 207-214.

[30] Ramos, A., Morgan, H., Green, N. G., Castellanos, A., *J. Phys. D-Appl. Phys.* 1998, *31*, 2338-2353.

[31] Das, C. M., Becker, F., Vernon, S., Noshari, J., Joyce, C., Gascoyne, P. R. C., *Analytical Chemistry* 2005, *77*, 2708-2719.

[32] LaLonde, A., Gencoglu, A., Romero-Creel, M. F., Koppula, K. S., Lapizco-Encinas, B. H., *Journal of Chromatography A* 2014, *1344*, 99-108.

[33] Prieto, J. L., Lu, J., Nourse, J. L., Flanagan, L. A., Lee, A. P., *Lab on a Chip* 2012, *12*, 2182-2189.

[34] Stubbe, M., Gimsa, J., *Colloids and Surfaces a-Physicochemical and Engineering Aspects* 2011, *376*, 97-101.

[35] Li, Y. B., Ren, Y. K., Liu, W. Y., Chen, X. M., Tao, Y., Jiang, H. Y., *Electrophoresis* 2017, *38*, 983-995.

[36] Liu, W. Y., Ren, Y. K., Shao, J. Y., Jiang, H. Y., Ding, Y. C., *J. Phys. D-Appl. Phys.* 2014, *47*.

[37] Stubbe, M., Gyurova, A., Gimsa, J., *Electrophoresis* 2013, *34*, 562-574.

[38] Gascoyne, P. R. C., Shim, S., Noshari, J., Becker, F. F., Stemke-Hale, K., *Electrophoresis* 2013, *34*, 1042-1050.

[39] Gascoyne, P. R. C., Wang, X. B., Huang, Y., Becker, F. F., *IEEE Trans. Ind. Appl.* 1997, *33*, 670-678.